PRAMANA
— journal of
physics

Vol. 53, No. 6
December 1999
pp. 951–961

Cosmic microwave background radiation anisotropies and data analysis

SHIV K SETHI
Mehta Research Institute, Chhatnag Road, Jhusi, Allahabad 211 019, India

Abstract. The theory of generation of CMBR temperature and polarization fluctuations is briefly reviewed. Also discussed is the present status of observations and the nature of future surveys.

Keywords. CMBR; large scale structure; cosmology.

PACS Nos 98.65 Dx; 98.80 Es; 98.70 Vc

1. Introduction

One of the major cornerstones of the big bang cosmology is the observed properties of the cosmic microwave background radiation (CMBR) [1,2]. CMBR is observed to be a black body to better than one part in two hundred thousand, which points to a hot and compact beginning of the Universe [3]. Another important property of CMBR is the observed anisotropy in its distribution which gives important clues on the way large scale structure formed in the Universe [4].

In inflationary paradigm the density perturbations are generated during the inflationary epoch and grow to yield the large scales structure we see at present (for a review see [5]). CMBR is generated at a redshift $\simeq 1100$ at the epoch of recombination [2]. If the matter was distributed completely homogeneously at the last scattering surface (LSS) the CMBR would have been totally isotropic. The small level of anisotropies present in CMBR carry information about the small level of inhomogeneities present in the matter at the epoch of recombination. For viable models of structure formation, the level of anisotropy in CMBR temperature is expected to be approximately one part on hundred thousand at angular scales from 180° to a few arc minutes [2].

COBE-DMR discovered CMBR the temperature anisotropies at angular scales $\geq 7^\circ$ in 1992 [4]. Following this discovery nearly 10 experiments have reported positive detection of anisotropies on angular scales varying from a few degrees to 10 arc minutes (for a comprehensive compilation of recent results see [6]). In addition to temperature anisotropies, a small level of polarization fluctuations are also generated at the LSS [7]. Though at present there are only upper limits on the polarization fluctuations [8,9], these which might be detected in not too distant future [10].

In §2 we present the physics for estimating the level of temperature and polarization anisotropies. In section §3, the problem of extracting the CMBR signal in the presence of pixel noise and foregrounds is addressed.

2. Statistical description of temperature and polarization anisotropies

Given a scalar field like temperature on every point on the sky or a small patch of it, it can be expanded in spherical harmonics:

$$T(\theta,\phi) = \sum_{l,m} a_l^m Y_l^m(\theta,\phi). \tag{1}$$

Using orthonormality of spherical harmonics, we can write

$$a_l^m = \int \mathrm{d}\Omega Y_l^{-m}(\theta,\phi) T(\theta,\phi). \tag{2}$$

The temperature (and polarization) fluctuations are a random field on the sky. If these fluctuations are caused by matter inhomogeneities generated during the inflationary epoch, then a generic prediction of inflation is that the fluctuations are a Gaussian random process. This greatly simplifies the analysis of the CMB fluctuation analysis because the only two relevant moments for a Gaussian random process is its mean ($= a_0^0$) and its variance. The variance is, after subtracting the mean, the two-point correlation function of the temperature anisotropies:

$$C(\theta_{12}) = \langle T(\theta_1,\phi_1) T(\theta_2,\phi_2)\rangle. \tag{3}$$

It is often more convenient to do the analysis in the $\{l,m\}$ space. The angular power spectrum is defined as:

$$\langle a_l^m a_{l'}^{-m'}\rangle = C_l \delta_{ll'} \delta_{mm'}. \tag{4}$$

It is related to the two-point correlation function in $\{\theta,\phi\}$ as:

$$C(\theta) = \sum_l \frac{(2l+1)}{4\pi} C_l P_l(\cos\theta). \tag{5}$$

Here $P_l(\cos\theta)$ is the Legendre polynomial of degree l. The aim of any CMBR experiment is to estimate C_l as it contains all the information of the underlying random process in the Gaussian limit.

CMBR polarization is generated by Thompson scattering which generates only linear polarization. Therefore, it can be expressed in term of Stokes parameter Q and U and the Stokes parameter V, which measures the circular polarization is always zero (for details see [11]). These Stokes parameters are defined with respect to the plane perpendicular to the line of sight and transform like a second-rank tensor field under rotation in that plane. This makes the statistical description of CMBR polarization considerably more difficult. Linear combinations $Q+iU$ and $Q-iU$ can be shown to transform like spin 2 and -2 objects, and therefore can be transformed in terms of spin-weighted spherical functions [14]:

$$\begin{aligned}(Q+iU)(\theta,\phi) &= \sum_{l,m} a_{2,l}^m {}_2Y_l^m(\theta,\phi)\\ (Q-iU)(\theta,\phi) &= \sum_{l,m} a_{-2,l}^m {}_{-2}Y_l^m(\theta,\phi)\end{aligned} \tag{6}$$

Here ${}_2Y_l^m$ and ${}_{-2}Y_l^m$ are spin-weighted spherical functions. This allows one to define rotationally invariant quantities, E and B. In spherical harmonic space, E and B are related to the Stokes parameter as:

$$a_{E,l}^m = -(a_{2,l}^m + a_{-2,l}^m)/2$$
$$a_{B,l}^m = i(a_{2,l}^m - a_{-2,l}^m)/2 \tag{7}$$

E and B in real space can be got by the spin-weighted transform of eq. (7). These quantities like temperature are scalars under rotations, and therefore eqs (3)–(5) can be used for describing their statistical properties. In general CMB data can give four quantities: C_l^T, C_l^E, C_l^{TE}, and C_l^B. C_l^{TE} gives the cross-correlation between temperature and the E-mode polarization. C_l^{TB} and C_l^{EB} are zero because B is pseudo-scalar.

3. Generation of temperature and polarization anisotropies

At LSS the density inhomogeneities are small, i.e. $\delta\rho/\rho_t \ll 1$. Here ρ_t correspond to the total background density while $\delta\rho$ is the fluctuation in any one of the components. In the standard CDM (sCDM) model, $\Omega_t \equiv \rho_t/\rho_c = \Omega_\gamma + \Omega_\nu + \Omega_{\rm CDM} + \Omega_B = 1$, where $\Omega_\gamma = 2.49 \times 10^{-5}\,{\rm h}^{-2}$, $\Omega_\nu = 1.7 \times 10^{-5}\,{\rm h}^{-2}$, $\Omega_B = 0.0125\,{\rm h}^{-2}$ are the contributions from photons, three massless neutrinos, and baryons respectively. In sCDM model, $h = 0.5$ and requiring $\Omega_t = 1$ gives $\Omega_{\rm CDM} \simeq 0.95$. Throughout this review, unless specified otherwise, the model used would be sCDM. Small level of inhomogeneities allows one to use the linear perturbation theory. In linearized theory, there are three sources of temperature anisotropies: (a) potential difference between the observer and the emitter (Sachs–Wolfe (SW) effect [12]). In sCDM, the main contribution to this effect arises from the potential difference between the LSS and present and the temperature fluctuation in any direction can be written as: $\Delta T/T(\hat{n}) = 1/3\Phi(\hat{n}, t_r)$, where $\phi(\hat{n})$ is the Newtonian potential associated with $\delta\rho_t$, and t_r is the time at the recombination. In various other variants of sCDM models, there can be substantial contribution from the time-variation of the potential (Integrated Sachs–Wolfe (ISW) effect [12]), (b) bulk velocity of baryons at LSS causes a perturbation in the photon temperature, $\Delta T/T(\hat{n}) = \mathbf{V_b}.\hat{n}/c$, and (c) intrinsic fluctuations. Initial conditions couple the fluctuations in photons to baryons. For adiabatic initial conditions, $\Delta T/T(\hat{n}) = 1/3\delta\rho_B/\rho_B$. Throughout this review we shall consider only adiabatic initial conditions.

Temperature (or polarization) fluctuations, $\Delta_T(\hat{n}, \vec{x})$, can be Fourier decomposed. In linear perturbation theory, different Fourier modes, $\Delta_T(\hat{n}, \vec{k})$ evolve independently of one another. Further assuming the perturbations to be axially symmetric around $\hat{k}$, i.e. $\vec{k}$ is parallel to z-axis, the fluctuations can be expanded in the angle $\mu = \cos\theta = \vec{k}.\hat{n}/k$,

$$\Delta_T(\hat{n}, \vec{k}) = \sum_l (2l+1)(-i)^l \Delta_{Tl}(k) P_l(\mu). \tag{8}$$

Here $\Delta_{Tl}(k)$ is the contribution of a given k to the mode l. A similar expansion is possible for polarization anisotropies.

The evolution of a Fourier component k of temperature and polarization fluctuations can be written as [11,13]:

$$\dot{\Delta}_T + ik\mu(\Delta_T + \Psi) = \dot{\Phi} + \dot{\kappa}\left\{-\Delta_T + \Delta_{T0} + i\mu V_b + \frac{1}{2}P_2(\mu)[\Pi]\right\}$$

$$\dot{\Delta}_P + ik\mu\Delta_P = \dot{\kappa}\left\{-\Delta_P + \frac{1}{2}[1 - P_2(\mu)]\Pi\right\}. \tag{9}$$

For simplicity the k dependence of the fluctuations has been suppressed. $\Pi = \Delta_{T2} + \Delta_{P2} + \Delta_{T0}$, 'dot' is time derivative with respect to conformal time, $\tau = \int \mathrm{d}t a_0/a$; $\dot{\kappa} = x_e n_e \sigma_T a/a_0$, x_e being the ionized fraction. These equations are written in Longitudinal gauge, and Φ and Ψ are the potential that represent the two scalar modes of perturbation (for details on gauge issues see [2]). Φ is the Newtonian potential introduced above. Several qualitative features of fluctuation evolution can be gleaned from these equations: In temperature fluctuations, one can identify the three sources of fluctuations, (a) SW and ISW effects are given by the terms proportional to Φ and Ψ and their time derivatives, respectively. We do not consider possible contributions from tensor modes in this review. In sCDM model $\Psi \simeq \Phi$, and the Newtonian potential Φ is independent of time and hence there is negligible contribution from ISW effect. However, ISW effect can be important when one needs to get the anisotropies at $10\,\%$ level [18], (b) the term proportional to V_b gives the contribution of Doppler shift to the anisotropies, and (c) Δ_{T0} gives the anisotropy from intrinsic fluctuations. The only source of polarization anisotropy is the quadrupole moment of temperature fluctuations. It is not surprising as the only way polarization can be induced at the LSS is by scattering of CMBR photons off electrons (Thomson scattering). And the angular dependence of Thomson scattering ensures that the non-zero polarization can only be generated if the photon distribution has a non-vanishing quadrupole.

To solve (9) one needs to know the evolution of baryon velocity and the two potentials Φ and Ψ. The evolution of baryon velocity in linearized theory is:

$$\dot{V}_b = -\frac{\dot{a}}{a}V_b + k\Psi + \frac{\dot{\kappa}}{R}(3\Delta_{T1} - V_b). \tag{10}$$

Here $R \equiv 3\rho_b/4\rho_\gamma$ is the ratio between baryonic and radiation (CMBR) densities. The evolution of Φ and Ψ is coupled very weakly to evolution of photon perturbations for $\tau \leq \tau_r$, τ_r being the conformal time at recombination. The reason for this weak coupling is that the potentials are determined by the perturbation in the dominant component at any time; around recombination, photons contribute $\simeq 5\,\%$ to the energy density of the Universe, and this contribution decreases as the time progresses as $(1+z)^{-1}$. Therefore if very accurate estimate of temperature anisotropies is not needed, eqs (9) and (10) do not influence the evolution of the potentials.

Several different methods have been tried to solve eqs (9) (for a review see [15]). In recent years efficient methods to get both exact and approximate solutions to eqs (9) have emerged. The approximate methods have turned out to be very useful for getting physical insight into the problem.

3.1 *Approximate solutions of perturbations: Temperature anisotropies*

For $\tau \ll \tau_r$, $\dot{\kappa}^{-1} \ll \tau$, i.e., the rate of Thomson scattering in the fully-ionized plasma far exceeds that of the expansion rate of the Universe. Equations (9) can be considerably

simplified at such epochs by expanding the equations as powers of $\dot{\kappa}$ (this is called the tight coupling approximation (TCA). The zeroth order term gives [16,17]:

$$\begin{aligned} \Delta_T &= \Delta_{T0} + i\mu V_b \\ \Delta_{T1} &= V_b/3, \quad \Delta_{Tl} = 0 \text{ for } l \geq 2. \end{aligned} \tag{11}$$

As the Universe expands the mean free path of photons increases due to dilution of baryons. As recombination approaches the mean free path increases very sharply because of the formation of hydrogen atoms, which leads to a breakdown in TCA. Around the epoch of recombination, $z \simeq 1100$, $\dot{\kappa}\tau \simeq 50$, if the entire plasma is assumed to be ionized. Therefore, TCA remains a fairly good approximation during most of recombination process and by expanding eq. (9) in powers of $\dot{\kappa}$ and retaining the three leading order terms (zeroth, first, and second) all the essential physics of the generation of the anisotropies is captured [17].

To set these ideas on firmer footing it is instructive to formally integrate (9), the solution can be written as:

$$\begin{aligned} (\Delta_T + \Psi) = & \int_0^{\tau_0} \mathrm{d}\tau e^{ik\mu(\tau-\tau_0)} \mathrm{e}^{-\kappa(\tau_0,\tau)} \\ & \times \left\{ \dot{\kappa} \left(\Delta_{T0} + \Psi + i\mu V_b + \frac{1}{2} P_2(\mu)[\Delta_{T2} + \Delta_{P2} + \Delta_{P0}] \right) - \dot{\Phi} + \dot{\Psi} \right\} \\ \Delta_P = & - \int_0^{\tau_0} \mathrm{d}\tau \mathrm{e}^{ik\mu(\tau-\tau_0)} \dot{\kappa} \mathrm{e}^{-\kappa(\tau_0,\tau)} \frac{1}{2} [1 - P_2(\mu)][\Delta_{T2} + \Delta_{P2} + \Delta_{P0}]. \end{aligned} \tag{12}$$

This can be further simplified and several qualitative features can be gleaned from these solutions. In TCA, the second moments of photon distribution can be dropped from the right hand side in the equation for temperature anisotropy. Further TCA allows one to write the baryon velocity term in terms of the first moment of the photon distribution (eq. (11)). In this approximation, the integrand for temperature fluctuation just contains the zeroth and first moment of Δ_T. TCA can be used to solve for these two moments: Expanding the first of eq. (9) in first power of $\dot{\kappa}$ and taking the zeroth and first moment give two linear differential equations for Δ_{T0} and Δ_{T1} which can be solved either analytically or numerically (for more details see [18,19]).

The visibility function, $v(\tau) = \dot{\kappa} \exp(-\kappa(\tau_0, \tau)$ multiplies all the terms in eq. (12), except the terms containing time derivatives of potentials (ISW term) in the first equation. This function is a sharply peaked function which can be approximated by a Gaussian with its peak at $z \simeq 1100$ and width $\delta z \simeq 80$. Therefore, the anisotropies seen at present are generated in a fairly small time span near recombination. This feature allows us, with TCA, to break the anisotropy generation process in two different epochs: (a) the width of the visibility function, during which TCA is assumed to be valid, (b) the free-streaming epoch which occurs when $\dot{\kappa}^{-1} \geq \tau$. This epoch last till the present. During the free-streaming epoch, the existing homogeneities at any linear scale get converted to anisotropies at smaller angular scales. It occurs because photon horizon H^{-1} is $\propto \tau^3$ while the physical length scales grow as $\propto \tau^2$. Assuming the visibility function to be a delta function and using (8) to take moments of the left hand side of eq. (12), the solution of the first of (12) can be written as:

$$\Delta_{Tl}(\tau_0) \simeq (\Delta_{T0} + \Psi)(\tau_r) j_l(k(\tau_0 - \tau_r) + \Delta_{T1}(\tau_r) F(l, k, \tau, \tau_r) + \int_{\tau_r}^{\tau^0} (\dot{\Psi} - \dot{\Phi}) j_l(\tau_0 - \tau_r) \mathrm{d}\tau. \quad (13)$$

Here $F(l, k, \tau, \tau_r) = 1/(2l+1)[l j_l(k(\tau_0 - \tau_r)) - (l+1) j_{l+1}(k(\tau_0 - \tau_r))]$. τ_r can be chosen to be any suitable time after the recombination at which the visibility function is small. However, to use TCA which breaks down very rapidly as the recombination occurs, the choice of τ_r should be early enough for TCA to be valid and late enough for the visibility function to have diminished sufficiently. If very accurate solutions are not needed, such a τ_r can always be found [18]. Equation (13) captures the essence of temperature anisotropy generation. $\Delta_{Tl}(\tau_0)$ is seen to be depend only on the first two moments of photon distribution at τ_r. These two moments can be calculated using TCA [18,19]. The spherical Bessel functions multiplying these two solutions just give the conversion of a given linear scale to an angular scale for any epoch. Further details which we have not talked about comes from expanding eq. (9) in second order in $\dot{\kappa}$. This gives the damping of anisotropies due to diffusion of photons in the imperfect photon-baryon fluid (Silk damping [20]). This diffusion process destroys anisotropies at small scales, which has to be taken into account. Also the width of last scattering surface wipes out anisotropies at scales smaller than the width (for details of how it is achieved in getting approximate solutions using TCA, see [18]).

The angular power spectrum can be obtained from squaring eq. (13), averaging, and integrating over all k:

$$C_l^T = \frac{2}{\pi} \int \mathrm{d}k k^2 \left|\Delta_{Tl}(k, \tau_0)\right|^2. \quad (14)$$

3.2 *Approximate methods: Polarization perturbations*

As seen in the second of eq. (9) the only source of polarization is the quadrupole moment of temperature perturbation. To zeroth order in TCA, only the zeroth and first moments of temperature distribution are non-vanishing (eq. (11)), and therefore in this approximation $\Delta_P = 0$. A non-vanishing source of polarization comes in the first order in $\dot{\kappa}$, in this approximation [21]:

$$\Delta_{T2} = \frac{8}{15} k \tau_r \Delta_{T1},$$
$$\Delta_{P0} = -\frac{5}{4} \Delta_{T2},$$
$$\Delta_{P2} = \frac{1}{4} \Delta_{T2}. \quad (15)$$

Following steps similar to getting eq. (13), one can obtain (for detailed derivation see [21]):

$$\Delta_P = 0.51 k \Delta_{T1}(\tau_r) \delta\tau_r (1 - \mu^2) \exp[ik\mu(\tau_0 - \tau_r)]. \quad (16)$$

Here $\delta\tau_r$ is the width of the visibility function. eq. (16) shows that polarization fluctuations are proportional to the dipole of temperature fluctuations, which we have seen above can

be determined using TCA. Our next aim is to obtain C_l^E, C_l^{TE} and C_l^B starting from this expression and using eq. (13) It can be shown that C_l^B vanishes for scalar perturbations [14]. The steps to reach C_l^E or C_l^{TE} from eq. (16) are tricky and the reader is referred to [14].

The approximate methods described above give all the essential physics of the process of generation of temperature and polarization fluctuations–acoustic oscillations of the baryon-photon fluid, SW and ISW effect, Silk damping, and fuzzing due to the finite width of LSS. In addition, these approximate analytic solutions uncover the dependence of the angular power spectra on various cosmological parameter (for more detail see [18,21,23]). These solutions can be used if better than 10% accuracy is not needed.

Exact solutions of eq. (9) also work around the philosophy of the approximate solutions using TCA. They involve a more careful integration over the width of visibility function, and up to 10 moments of photon distribution are solved till τ_r, the time after which the solutions can be free-streamed, etc. A very fast numerical code which calculates various angular power spectra to 1% accuracy has been developed and is publicly available (for details see [22]). In figure 1a we show the level of the signals expected in sCDM model using the package CMBFAST.

4. CMBR observations: Present status and future prospects

In figure 1b we give a compilation of some of the most important results obtained so far, along with the predictions of two theoretical models; see [6] for a more complete compilation till 1997 end.

Although it is still early to choose the most favoured theoretical model from CMBR observations, it is possible to glean broad features suggested by the observations so far. The sCDM models seems to be inconsistent with the observed values from Saskatoon and Python experiments around $l = 200$. A better fit to data is seen to be a flat Universe with $\Omega_\Lambda = 0.7$, $\Omega_m = 0.25$, $\Omega_B = 0.05$, and $h = 0.5$. Another qualitative feature of observations is the position of peak of the observed anisotropies. It is seen to lie above the theoretical predictions of flat Universes. In an open (closed) Universe, the theoretical peak would shift to right (left), in disagreement with observations.

Detailed comparison between observations and theoretical predication has been performed by several authors in recent years [6,24,25]. A joint analysis of CMBR observations and SN1a data at high redshifts, which is giving independent evidence of a non-zero cosmological constant [26], suggest that the Universe is nearly flat with $\Omega_\Lambda \simeq 0.65$ [24]. The COBE-DMR results are also consistent with the observed galaxy distribution at the present epoch for some variants of sCDM model [27]. This supports the view that the galaxies arise from gravitational instability and that we might be very close to pin-pointing the exact model of their formation.

4.1 *Future observations*

What more can we learn from the study of CMBR anisotropies? It has been argued that the study of CMBR anisotropies is one of the cleanest ways to determine nearly 10

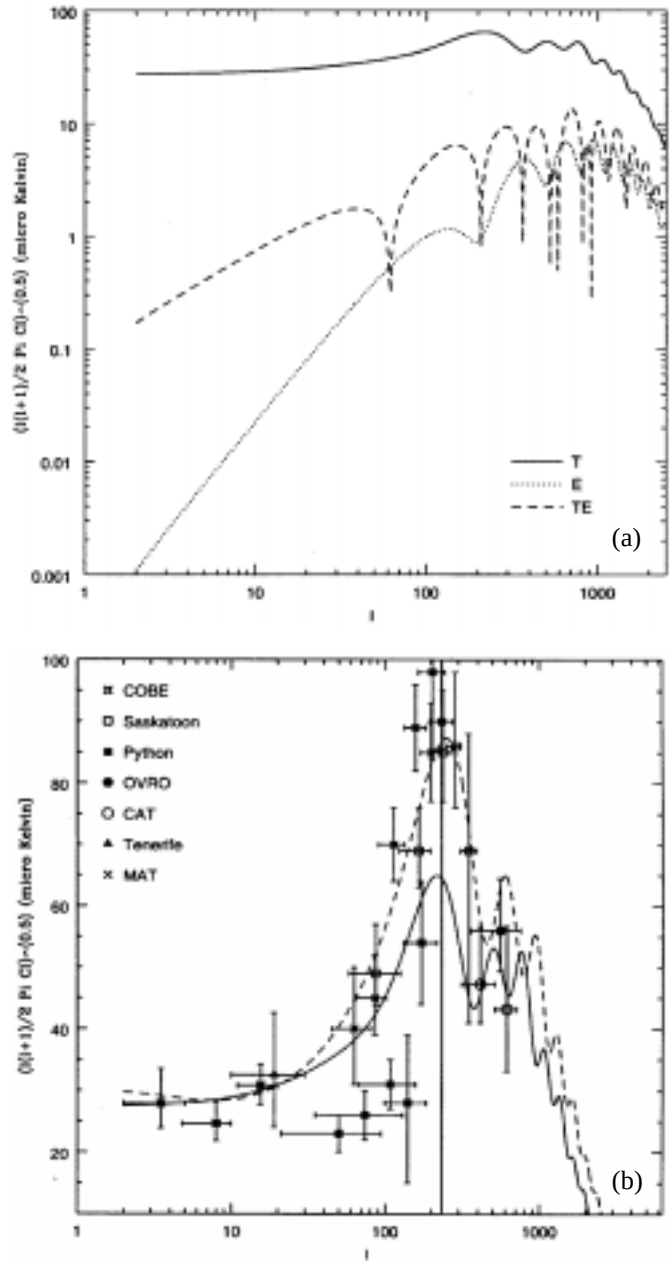

Figure 1. (**a**) Left Panel:CMBR anisotropies expected in sCDM model based on the package CMBFAST [22]. **(b)** Right Panel: Temperature anisotropy observations vis-a-vis theoretical predictions. The observations shown are: COBE [37], Saskatoon [9], Python [38], CAT [39], OVRO [40], Tenerife [41], and MAT [42]. Also shown are the theoretical predictions of sCDM (solid line) and ΛCDM model with $\Lambda = 0.7$ (dashed line).

cosmological parameters [28,29]. It has been shown that the future satellite missions can even achieve this to a few percent accuracy if both temperature and polarization information is available [30].

The main sources of uncertainties in estimating the power spectra of CMBR is the experimental noise, galactic and extragalactic foreground (we neglect the atmospheric foreground in our discussion), and the sample variance. Assume an experiment that is not hampered by foregrounds and it has Gaussian experimental noise which is uncorrelated between pixels. For such a case the CMBR power spectra C_l estimated from data can be approximated as a Gaussian random field with variance:

$$\Delta C_l = \left[\frac{2}{(2l+1)f_{\rm sky}}\right]^{1/2} \left(C_l + w^{-1}W_l^{-1}\right). \tag{17}$$

Here C_l is the underlying power spectra, $f_{\rm sky}$ is the fraction of sky covered in the experiment, and W_l is the experimental beam. $w^{-1} = \sigma^2_{\rm pix}\Omega_{\rm pix}/T_0^2$ is the pixel-area independent measure of noise for an experiment, where $\sigma^{\,2}_{pix}\delta_{ij} \equiv \langle \Delta T_i^{\rm noise} \Delta T_j^{\rm noise}\rangle$ is the variance of pixel noise, $\Omega_{\rm pix} = \theta^2_{\rm fwhm}$ is the area of a pixel, $T_0 = 2.726\,{\rm K}$ is the CMBR temperature. To calculate w^{-1}, consider an experiment that has a pixel sensitivity $s\sqrt{\rm sec}$ then $\sigma_{\rm pix} = s/\sqrt{t_{\rm pix}}$, where $t_{\rm pix}$ is the duration for which a pixel is observed. If the total time of observations is $t\,{\rm seconds}$ and a fraction $f_{\rm sky}$ of the sky is observed, $t_{\rm pix} = t \times \Omega_{\rm pix}/(4\pi f_{\rm sky})$. Taking numbers typical for a future satellite experiment: $s \simeq 100\,\mu{\rm k}$, $t = 3\times 10^7\,{\rm sec}$, and $f_{\rm sky} = 1$, $w^{-1} \simeq 10^{-15}$. (For comparison the four-year COBE maps had $w^{-1} \simeq 1.2\times 10^{-12}$.) W_l generally depends on observing strategy, for all-sky satellite experiments it is generally well approximated as a Gaussian, $\exp(-\sigma_b^2 l^2)$, σ_b being width of the experimental beam.

In eq. (17), the first term gives the error from sample variance. It comes from the fact that there are only $2l+1$ independent modes of C_l on the entire sky for any l, so a minimum error of $\sqrt{1/((2l+1)f_{\rm sky})}$ is expected on estimating C_l irrespective of the precision of measurement. For large l this error can be significantly reduced by covering a larger area of the sky. So far all the experiments, apart from COBE, cover only a very small fraction of the sky, which gives a large sample variance as well as w^{-1}. Therefore the aim of future experiments is, apart from greater pixel sensitivity, is to (a) cover a larger part of the sky, and (b) map the sky in a wide range of frequencies. This is to reduce contamination from foregrounds (see below).

Several new ground-based (both single dish and interferometric), balloon-based, and satellite experiments are currently either already operating or are scheduled to start functioning in near future. For a comprehensive list of future surveys and relevant web sites, see [31]. For a recent update on the on-going balloon experiment MAXIMA see [32].

As the future experiments will cover a larger area of the sky at better angular resolution and will have greater frequency coverage, the amount of data from these future missions would be unprecedented. For example, the future balloon mission TopHat will cover 1800 square degrees at any frequency with an angular resolution of $0.3\,{\rm degree}$, which means nearly 20000 independent pixels (compare it with COBE-DMR which had $\simeq 6000$ pixels). Future satellite missions, MAP and Planck will cover the entire sky with angular resolution even better than this and the expected number of pixels for these experiments is $\geq 10^6$ for any frequency channel. Getting useful information out of such huge data sets is one of the major challenges to the future CMB surveys [33].

Future satellite missions MAP and Planck will also have capability to detect polarization [34]. The error in the estimation of the polarization power spectra and temperature-polarization cross-correlation can be written in the form of eq. (17), and it has been shown that future surveys will achieve the noise levels and sky coverage required to detect this signal, if the effect of foregrounds can be neglected [14].

4.2 *Foregrounds*

Apart from the pixel noise, galactic and extragalactic foregrounds are the major obstacles in extracting the primordial signal from the observed sky. The pixel noise can be reduced by integrating longer or making more sensitive instruments but removal of foreground requires an entirely different strategy. The foreground differ from CMBR in both their spectral dependence and spatial distribution. Therefore almost all reliable CMBR experiments are multi-frequency. For example, COBE had three frequency channels: $30\,\mathrm{GHz}$, $53\,\mathrm{GHz}$, and $90\,\mathrm{GHz}$. The lowest frequency channel was dominated by galactic foreground free-emission and synchrotron and its aim was to monitor and remove foregrounds from the higher frequency channels which were dominated by CMBR signal.

Several methods have been suggested to clean the foreground contamination. It has been argued that the best method is based on multi-frequency Weiner filtering as it takes into account both the spectral and spatial difference between the CMBR and foregrounds [35]. It appears that the performance of the future multi-frequency satellite will not be significantly affected by the foregrounds for the detection of temperature anisotropies.

Polarization foregrounds are more difficult to model [36]. Recent studies show that though the foreground might seriously hamper the detection of polarization signal using MAP, Planck should make a clear detection of this signal [10].

References

[1] S Weinberg, *Gravitation and Cosmology* (Wiley, New York, 1972)
[2] J R Bond, in *Cosmology and large scale structure*, Les Houches proceedings, edited by R Schaeffer *et al* (1996)
[3] D J Fixsen, *et al*, *Astrophys. J.* **473**, 576 (1996)
[4] G Smoot *et al*, *Astrophys. J.* **396**, L1 (1992)
[5] V F Mukhanov, H A Feldman and R H Brandenberger, *Phys. Rep.* **215**, 203 (1992)
[6] C H Lineweaver and Barbosa, *Astrophys. J.* **496**, 624 (1998)
[7] M Rees, *Astrophys. J.* **153**, L1 (1968)
[8] M Lubin and G Smoot, *Astrophys. J.* **273**, L1 (1983)
R B Partridge, J Nowakowski and H M Martin, *Nature* **331**, 146 (1988)
[9] C B Netterfield *et al*, *Astrophys. J.* **474**, 47 (1997)
[10] F R Bouchet, S Prunet and S K Sethi, astro-ph/9809353 (MNRAS, in press) (1998)
[11] S Chandrasekhar, *Radiative processees* (Dover, New York, 1960)
[12] R K Sachs and A M Wolfe, *Astrophys. J.* **147**, 73 (1968)
[13] J R Bond and G Efstathiou, *Astrophys. J.* **285**, L85 (1984)
J R Bond and G Efstathiou, *Mon. Not. R. Astron. Soc.* **226**, 665 (1987)
[14] M Zaldarriaga and U Seljak, *Phys. Rev.* **D55**, 1830 (1997)
M Kamionkowski, A Kosowsky and A Stebbins, *Phys. Rev.* **D55**, 7368 (1997)

[15] G Efstathiou, in *Physics of the early Universe*, edited by A Heavens *et al* (1990)
[16] P J E Peebles and J T Yu, *Astrophys. J.* **162**, 815 (1970)
[17] P J E Peebles, *The large scale structure of the Universe*, Princeton University Press, Princeton, 1980)
[18] W Hu and N Sugiyama, *Astrophys. J.* **444**, 489 (1995)
[19] U Seljak, *Astrophys. J.*, **435**, L87 (1994)
[20] J Silk, *Astrophys. J.* **151**, 459 (1968)
[21] M Zaldarriaga and D D Harari, *Phys. Rev.* **D52**, 3276 (1995)
[22] U Seljak and M Zaldarriaga, *Astrophys. J.* **489**, 437 (1996)
[23] W Hu and N Sugiyama, *Astrophys. J.* **471**, 542 (1996)
[24] G Efstathiou *et al*, astro-ph/9812226, (1998)
[25] M Tegmark, astro-ph/9809201, (1998)
C Lineweaver, *Astrophys. J.* **505**, L69 (1998)
[26] S Perlmutter *et al*, astro-ph/9812133, (1998)
[27] G Efstathiou, J R Bond and S D M White, *Mon. Not. R. Astron. Soc.* **258**, 1 (1992)
[28] L Knox, *Phys. Rev.* **D52**, 4307 (1995)
[29] G Jungman, M Kamionkowski, A Kosowsky and D N Spergel, *Phys. Rev.* **D54**, 1332 (1996)
[30] M Zaldarriaga, D N Spergel and U Seljak, *Astrophys. J.* **488**, 1 (1997)
S Prunet, S K Sethi and F R Bouchet, submitted for publication to *Mon. Not. R. Astron. Soc.* (1999)
[31] L Page, in *Generation of large scale cosmological structure* (Erice, Sicily, 1996)
[32] A T Lee *et al*, astro-ph/9903244, (1999)
[33] J Borrill, astro-ph/9903204 (1999)
J R Bond *et al*, astro-ph/9903166, (1999)
[34] For details see http://map.gsfc.nasa.gov and
http://astro.estec.esa.nl/SA-general/Projects/Planck
[35] M Tegmark and G Efstathiou, *Mon. Not. R. Astron. Soc.* **281**, 1297 (1996)
F R Bouchet and R Gispert, astro-ph/9903176, (1999)
[36] S Prunet, S K Sethi, F R Bouchet and M-A Miville–Deschênes, *Astron. Astrophys.* **339**, 187 (1998)
[37] G Hinshaw *et al*, *Astrophys. J.* **464**, L17 (1996)
[38] K Coble *et al*, astro-ph/9902195, (1999)
[39] J Baker *et al*, in *Particle physics and early Universe* (Cambridge, 1997)
[40] E M Leitch *et al*, astro-ph/9807312, (1998)
[41] C M Gutiérrez *et al*, *Astrophys. J.* **480**, L83 (1997)
[42] E Torbet *et al*, astro-ph/9905100, (1999)